

Article

Effect of A-/B-site Doping on Oxygen Non-Stoichiometry, Structure characteristics, and O₂ Releasing Behavior of La_{1-x}Ca_xCo_{1-y}Fe_yO_{3-δ} Perovskites

Qiuwan Shen ¹, Shian Li ¹, Guogang Yang ^{1,*}, Bengt Sundén ^{2,*} and Jinliang Yuan ^{3,*}

¹ Marine Engineering College, Dalian Maritime University, Dalian 116026, China; shenqiuwan@dlnu.edu.cn (Q.S.); lishian@dlnu.edu.cn (S.L.)

² Department of Energy Sciences, Lund University, 22100 Lund, Sweden

³ Faculty of Maritime and Transportation, Ningbo University, Ningbo 315211, China

* Correspondence: yanggg@dlnu.edu.cn (G.Y.); Bengt.Sunden@energy.lth.se (B.S.); yuanjinliang@nbu.edu.cn (J.Y.)

Received: 28 December 2018; Accepted: 24 January 2019; Published: 28 January 2019



Abstract: Oxy-fuel combustion is one of the proposed technologies with the potential to achieve zero CO₂ emission. La_{1-x}Ca_xCo_{1-y}Fe_yO_{3-δ} (LCCF) perovskites are promising materials with high selectivity for oxygen. In this study, the oxygen non-stoichiometry of perovskites LCCF was investigated by means of iodometric titration. LCCF was prepared using the liquid citrate method, and the phase structures were identified by X-ray diffraction. Fixed-bed experiments were performed to study the oxygen desorption performance of LCCF. The oxygen deficiency of LCCF increased with increasing Ca molar content of A site, but the value of δ of LCCF with increasing Fe molar content in B site is nearly constant. Experimental observation demonstrated that the O₂ release amount of LCCF does not depend on oxygen non-stoichiometry δ generated from A-site doping. At the same time, doping Fe in B site has an obvious impact on the oxygen desorption amount.

Keywords: CO₂ capture; perovskites; oxygen non-stoichiometry; crystal structure; oxygen release

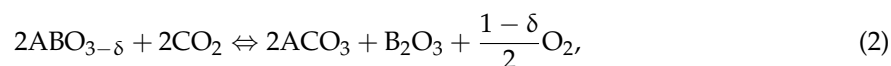
1. Introduction

In the combustion of fossil fuels, carbon dioxide emissions into the atmosphere lead to global warming [1–3]. Oxy-fuel combustion is one of the proposed technologies that has the potential to achieve a zero CO₂ emission. One of the key barriers for the implementation of oxy-combustion, however, is the cost of producing the oxygen. Cryogenic air-separation is an available method that has a major drawback—high energy consumption. Therefore, a new application of the perovskite metal oxides is to use them as sorbents in high-temperature sorption processes for air separation to produce O₂-enriched CO₂ stream [4,5].

Recently, perovskites have been extensively studied in applications like solid oxide fuel cells, oxygen-permeable membranes, gas sensors, catalysts, and photocatalytic materials [6–9]. Perovskite-type metal oxides have the general formula ABO₃; if A and/or B sites are substituted with lower valent cations, some oxygen ions are removed from the lattice in order to maintain charge neutrality, thereby giving rise to oxygen non-stoichiometry [10]. Perovskite metal oxides exhibit extremely high selectivity for oxygen due to the existence of oxygen vacancy. This is mainly because the A-site doping alkaline earth metal ions increase the concentration of oxygen vacancies, and the B-site doping transition metal ions produce mixed valence. Thus, their synergy improves the mixed ionic-electronic conductivity. Much research has been conducted to understand perovskite oxides

as oxygen-selective membranes. However, for oxygen production application, this technology faces major challenges in the manufacturing and stability of the membranes [11].

Lin et al. illustrated a high-temperature oxygen sorption process based on a perovskite-type sorbent to produce an O₂-enriched CO₂ stream for oxy-fuel combustion technology [12]. The perovskite-based oxygen production process has been reported in our previous study [1]. The reversible oxygen sorption and desorption process of perovskites is described below [13]:



where V_{O} is the oxygen vacancy, and $\text{O}_{\text{O}}^{\times}$ and h^{\cdot} denote lattice oxygen and electronic-hole, respectively.

The concentration of oxygen vacancies, which is important for oxygen adsorption and desorption processes, is characterized by oxygen non-stoichiometry of perovskites. If the cationic component is determined, the structure and properties of perovskites only depend on oxygen non-stoichiometry. Therefore, oxygen non-stoichiometry plays an important role in the capability of perovskites.

Currently, thermogravimetric analysis and iodometric titration are mainly used to measure oxygen non-stoichiometry. Teraoka [14] and co-authors developed a model, based on the defects in thermodynamic equilibrium, to describe oxygen non-stoichiometry in perovskite-type oxygen membranes. Yang et al. [15] used an empirical formula to describe the relationship between oxygen non-stoichiometry and the oxygen partial pressure. Cherepanov [16] found that in the case of constant temperature and oxygen partial pressure, oxygen non-stoichiometry of $\text{La}_{0.4}\text{Sr}_{0.6}\text{Co}_{1-y}\text{Fe}_y\text{O}_{3-\delta}$ ($y = 0.2$ and 0.4) increased by increasing Co-doping. When the A-site was doped with lower valence metal ions (in order to maintain charge neutrality and then induce the oxidation of Fe^{3+} and Co^{3+}), this led to the formation of oxygen vacancies. Oxygen non-stoichiometry increased with the increasing doping of low-valence metal ions.

Most of the above research works focused on oxygen non-stoichiometry with respect to oxygen partial pressure and temperature in oxygen-permeable membranes. However, there are few studies about oxygen non-stoichiometry and the oxygen-releasing performance of perovskite-type metal oxides that can be used for producing O₂-enriched CO₂ streams at a high temperature.

Iodometric titration [17,18] is easy to operate and can accurately measure oxygen non-stoichiometry. Therefore, oxygen non-stoichiometry of $\text{La}_{1-x}\text{Ca}_x\text{Co}_{1-y}\text{Fe}_y\text{O}_{3-\delta}$ ($x = 0.2, 0.5, 0.8$; $y = 0.2, 0.5, 0.8$) was measured using iodometric titration in this paper. Fixed-bed experiments were conducted to study the performance of oxygen desorption of perovskite oxides. Furthermore, the main purpose of this research is to study the influence of A-/B-site doping on oxygen non-stoichiometry, structure, and the performance of oxygen desorption of $\text{La}_{1-x}\text{Ca}_x\text{Co}_{1-y}\text{Fe}_y\text{O}_{3-\delta}$.

2. Experimental Methods

2.1. Sample Synthesis and Characterization

$\text{La}_{1-x}\text{Ca}_x\text{Co}_{1-y}\text{Fe}_y\text{O}_{3-\delta}$ (LCCF) was prepared by the liquid citrate method [19]. The phase composition of the samples was determined by X-ray diffraction (XRD, PANalytical B.V.) with Cu K α radiation ($\lambda = 0.1542$ nm) and a 2θ range of $20\text{--}70^\circ$ with a scanning step of 0.02° .

For the study of A-site doping of $\text{La}_{1-x}\text{Ca}_x\text{Co}_{1-y}\text{Fe}_y\text{O}_{3-\delta}$, X was changed from 0.2 to 0.8 with an interval of 0.3 and Y was fixed at 0.5. For the study of B-site doping of $\text{La}_{1-x}\text{Ca}_x\text{Co}_{1-y}\text{Fe}_y\text{O}_{3-\delta}$, X was fixed at 0.5 and Y was changed from 0.2 to 0.8 with an interval of 0.3. For example, LCCF2855 means $\text{La}_{0.2}\text{Ca}_{0.8}\text{Co}_{0.5}\text{Fe}_{0.5}\text{O}_{3-\delta}$, and LCCF5582 means $\text{La}_{0.5}\text{Ca}_{0.5}\text{Co}_{0.8}\text{Fe}_{0.2}\text{O}_{3-\delta}$.

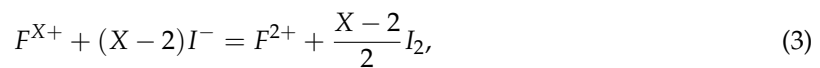
2.2. Measurements of Oxygen Stoichiometry

2.2.1. Iodometric Titration

Iodometric titration was performed via the reduction of I_2 and the oxidation of I^- to evaluate the oxygen content. In the La-Ca-Co-Fe oxides, iodide reduced any B-site ions (B^{3+} , B^{4+}) present to B^{2+} and was simultaneously oxidized to form I_2 . The amount of I_2 released was quantified via redox titration with $Na_2S_2O_3$ solution. Oxygen non-stoichiometry was then determined based on the amount of I_2 formed.

Certain amounts of sample were weighed accurately and then dissolved into an aqueous hydrochloric acid with excess KI. Then, B-site ions reacted with I^- and released I_2 in the solution. The consumption volume of the $Na_2S_2O_3$ solution was recorded. Then, the average valence of B-site and oxygen non-stoichiometry δ was calculated by the reaction equation and the charge neutrality principle.

F represents the B-site ions Co and Fe in a sample, and, assuming the average valence of F is X , then the titration reaction equation is as follows:



Assuming the molar mass of the sample is M , the average valence in A site is Y , and the sample mass is m . C represents the concentration of $Na_2S_2O_3$, and the total consumption volume of $Na_2S_2O_3$ solution is recorded as ΔV . Then, oxygen non-stoichiometry δ can be calculated by

$$\delta = \frac{(4 - Y)m - Mn}{2m - 16n}, \quad (5)$$

where $n = C \times \Delta V$.

2.2.2. Measurements of δ

An m (mg) amount of sample was weighed accurately. An excess of potassium iodide (KI) and 6 mL of 6 N HCl were added. Some distilled water was added to completely dissolve the sample. When the solution was cooled, the present iodine was titrated with standardized 0.01 mol/L $Na_2S_2O_3$. When the solution began to change color, 2 drops of 1% starch were added, and titration was continued until the dark blue color disappeared. The consumed volume of $Na_2S_2O_3$ was recorded, and then the amount of oxygen was calculated.

2.3. Oxygen Adsorption/Desorption Experiments

Oxygen adsorption/desorption experiments of synthetic perovskites were performed in the fixed-bed reactor, as shown in Figure 1, where 1 g of LCCF powder was packed in the quartz reactor. The flow rates of adsorption/desorption streams were 100 ml/min and 50 ml/min, respectively. The adsorption and desorption temperatures were 800 °C and 850 °C, respectively. The detailed experimental process can be found in our previous study [1,2].

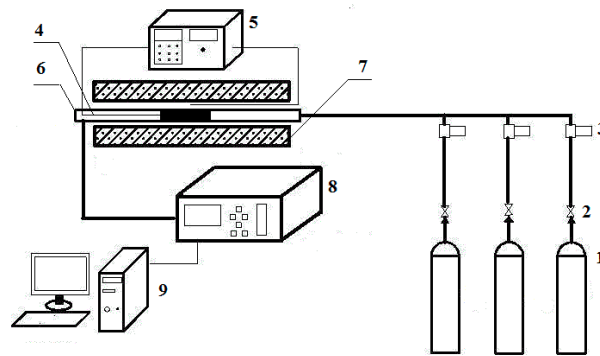


Figure 1. Diagrammatic sketch of a fixed-bed reaction system: (1) Gas cylinder, (2) valve, (3) mass flow controller, (4) thermocouple, (5) temperature controller, (6) quartz reactor, (7) horizontal tube furnace, (8) gas analyzer, and (9) data acquisition system.

3. Results and Discussion

3.1. XRD Analysis and Tolerance Factor

XRD patterns of the prepared perovskites powders are shown in Figure 2. The main characteristic peaks of all the samples showed that they were perovskite structures. The crystalline sizes of the samples (by the Scherer method) were in the range of 30–60 nm.

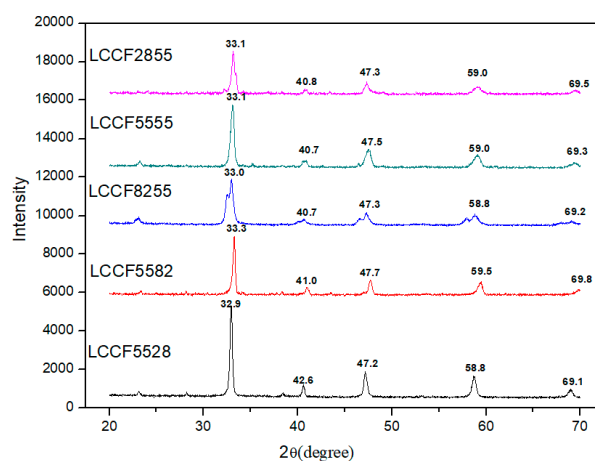


Figure 2. X-ray diffraction (XRD) patterns of fresh $\text{La}_{1-x}\text{Ca}_x\text{Co}_{1-y}\text{Fe}_y\text{O}_{3-\delta}$ powders.

The XRD pattern of $\text{La}_{0.8}\text{Ca}_{0.2}\text{Co}_{0.5}\text{Fe}_{0.5}\text{O}_{3-\delta}$ (LCCF8255) was only slightly different from the others. Its main peaks exhibited a broader area and split, which were caused by La-doping—as La is a trivalent ion, and Ca is a divalent one. Thus, LCCF8255 had a bigger A-site charge imbalance, which led to a distorted structure.

Tolerance factors (TF) reflect the degree of distortion of the crystal structure. For ABO_3 perovskite-type structure, TF was calculated by [20] as follows:

$$t = (r_A + r_B) / \sqrt{2}(r_B + r_O), \quad (6)$$

where r_A is the A-site ion radius, r_B is the B-site ion radius, and r_O is the oxygen ion radius.

Generally, materials can keep a perovskite-type structure when t is in the range of 0.75–1.00. It is thought that materials have the most stable cubic perovskite structure when $t = 1$.

For A-site/B-site perovskite doped with $\text{A}_x\text{A}'_{1-x}\text{B}_y\text{B}'_{1-y}\text{O}_{3-\delta}$, the value of t can be calculated by

$$t = [xr_A + (1-x)r_{A'} + r_O] / \sqrt{2}[yr_B + (1-y)r_{B'} + r_O]. \quad (7)$$

Table 1 lists the radii of the doping ions and t value of the samples, respectively. The La and Ca ions' radii in A-site are very approximate however they have different valence. In the B-site, the Fe ion's radius was almost equal to the Co ion's radius, but they had the same valence. The t values for all doping samples were close to 1. Thus, all of them had a perfect perovskite structure, where t of LCCF5582 was closest to 1.

Table 1. Radii of the doping ions and t values of prepared samples.

Ions	Ionic Radii (Å)	Oxides	t
La ³⁺	1.36	LCCF8255	1.0008
Ca ²⁺	1.34	LCCF5555	0.9986
Co ³⁺	0.545	LCCF2855	0.9964
Fe ³⁺	0.55	LCCF5582	0.9994
		LCCF5528	0.9979

Figure 3 shows the XRD pattern of La_{0.5}Ca_{0.5}Co_{0.8}Fe_{0.2}O_{3-δ} (LCCF5582) after desorption with CO₂ gas at 850 °C in 1 atm. The XRD pattern of solid products from the carbonation reaction for LCCF5582 showed the main characteristic peaks of La₂O₃ and SrCO₃, along with the remaining CoO and Fe₂O₃, and basically no perovskite phase.

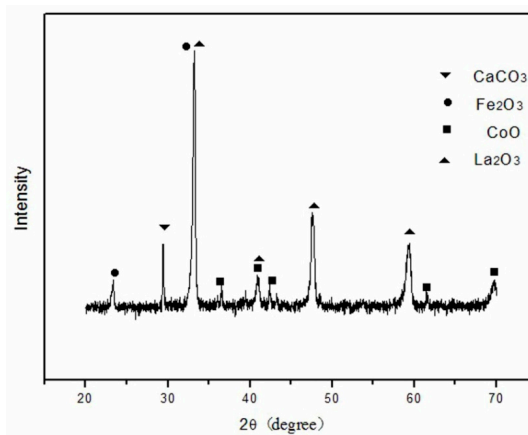


Figure 3. XRD patterns of La_{0.5}Ca_{0.5}Co_{0.8}Fe_{0.2}O_{2.698} after complete carbonation at 850 °C.

3.2. Oxygen Non-Stoichiometry

The oxygen non-stoichiometry δ of La_{1-x}Ca_xCo_{0.5}Fe_{0.5}O_{3-δ} ($x = 0.2, 0.5, 0.8$) and La_{0.5}Ca_{0.5}Co_{1-y}Fe_yO_{3-δ} ($y = 0.2, 0.5, 0.8$) were determined by iodometric titration. For each sample, the experiment was done three times to reduce experimental errors, and the results of three experiments were averaged to obtain the final results, as shown in Figures 4 and 5.

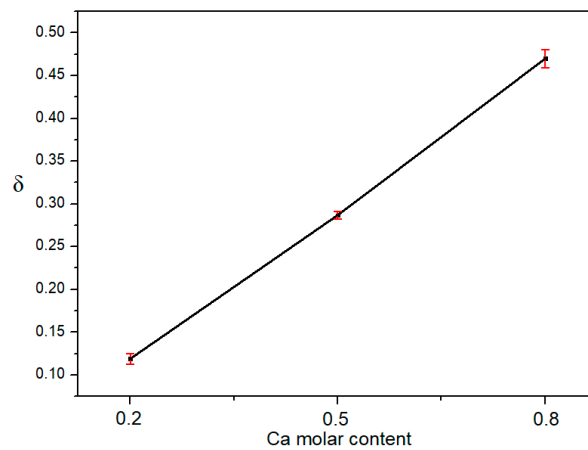


Figure 4. The Oxygen non-stoichiometry of $\text{La}_{1-x}\text{Ca}_x\text{Co}_{0.5}\text{Fe}_{0.5}\text{O}_{3-\delta}$ ($x = 0.2, 0.5, 0.8$).

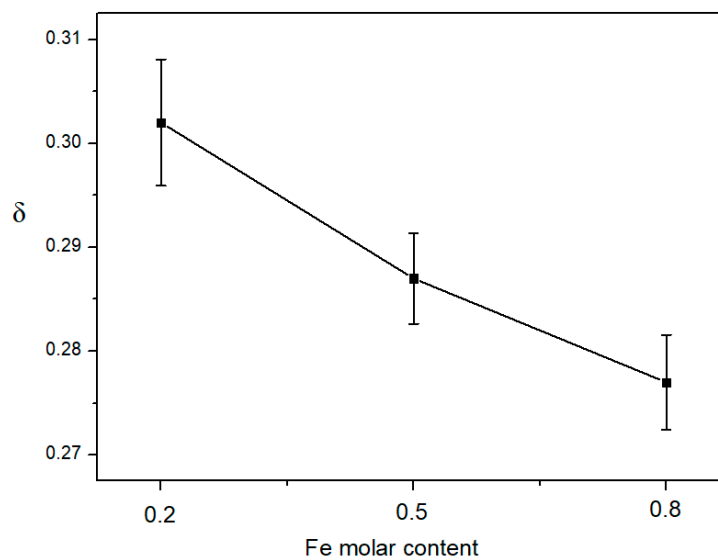


Figure 5. The oxygen non-stoichiometry of $\text{La}_{0.5}\text{Ca}_{0.5}\text{Co}_{1-y}\text{Fe}_y\text{O}_{3-\delta}$ ($y = 0.2, 0.5, 0.8$).

Figure 4 shows that the Ca molar content had a significant effect on the oxygen non-stoichiometry of $\text{La}_{1-x}\text{Ca}_x\text{Co}_{0.5}\text{Fe}_{0.5}\text{O}_{3-\delta}$. The value of δ increased with increasing Ca molar content, and the maximum value of δ was 0.47. As is known, the Ca^{2+} radius is smaller than La^{3+} ; thus, the cell size of $\text{La}_{1-x}\text{Ca}_x\text{Co}_{0.5}\text{Fe}_{0.5}\text{O}_{3-\delta}$ decreased with increasing Ca molar content. This promoted oxygen defect formation and reduced the oxygen ion diffusion activation energy in the crystal structure. Meanwhile, the lower valence of Ca^{2+} encouraged oxygen ions to escape from the lattice in order to maintain electrical neutrality when the Ca molar content increased.

Figure 5 shows that the oxygen non-stoichiometry δ of $\text{La}_{0.5}\text{Ca}_{0.5}\text{Co}_{1-y}\text{Fe}_y\text{O}_{3-\delta}$ decreased slightly with increasing Fe content. It is known that the Fe–O bond energy ($408.8 \pm 13\text{KJ/mol}$) is larger than that of Co–O ($368 \pm 21\text{KJ/mol}$). Thus, it was more difficult to form oxygen vacancies in the perovskite with increasing Fe molar content. Moreover, compared to the Fe ion, Co was more adaptable in relocating to a lower valence. Therefore, in order to balance the valence, perovskites with a higher molar content of Co formed more oxygen vacancies.

Ca-doping significantly affected the oxygen vacancy concentration of $\text{La}_{1-x}\text{Ca}_x\text{Co}_{1-y}\text{Fe}_y\text{O}_{3-\delta}$, and oxygen non-stoichiometry δ was more sensitive to Ca-doping. In contrast, Fe molar content had little influence on oxygen non-stoichiometry δ of $\text{La}_{1-x}\text{Ca}_x\text{Co}_{1-y}\text{Fe}_y\text{O}_{3-\delta}$.

3.3. Oxygen Adsorption/Desorption Experiments of $La_{1-x}Ca_xCo_{1-y}Fe_yO_{3-\delta}$

Five LCCF samples of different stoichiometry (LCCF8255, LCCF5555, LCCF2855, LCCF5582, and LCCF5528) were synthesized by the liquid citrate method, and the fixed-bed reactor was used to study the oxygen desorption performance of LCCF. The adsorption temperature and desorption temperature were 800 °C and 850 °C, respectively. The oxygen desorption curves of LCCF perovskite with A-site Ca-doping are given in Figure 6. There was a plateau-like peak at about 500s in the initial stage of the exposure to CO₂, which may have been caused by the reversible defect reaction (1). The result agreed with the study by Yang et al. [4]. Then, the O₂ concentration increased sharply due to the carbonation reaction. For LCCF8255, there was a maximum oxygen concentration of about 2.2%. The carbonation reaction of LCCF8255 is as follows:

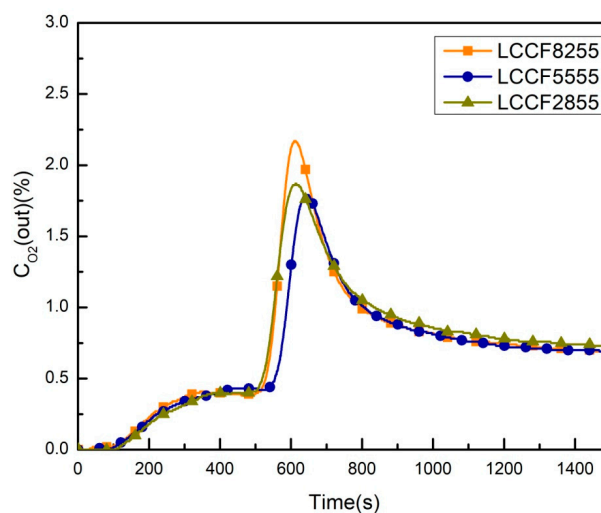


Figure 6. Oxygen desorption curves of $La_{1-x}Ca_xCo_{0.5}Fe_{0.5}O_{3-\delta}$ ($x = 0.2, 0.5, 0.8$).

Table 2 shows the oxygen desorption amount of $La_{1-x}Ca_xCo_{0.5}Fe_{0.5}O_{3-\delta}$ with different Ca molar contents. As seen in Table 3, along with the increasing amount of Ca-doping in $La_{1-x}Ca_xCo_{0.5}Fe_{0.5}O_{3-\delta}$, the oxygen desorption amount decreased slightly before increasing. This result showed that Ca-doping in the A-site does not have significant effect on the oxygen desorption amount of $La_{1-x}Ca_xCo_{0.5}Fe_{0.5}O_{3-\delta}$. This can also be seen from the carbonation reaction equation as follows:

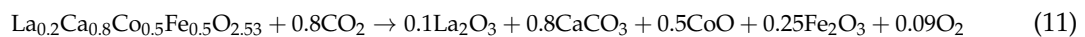
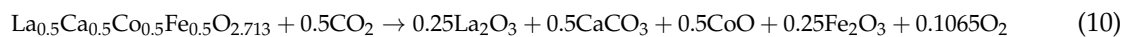


Table 2. Oxygen desorption amount of $La_{1-x}Ca_xCo_{0.5}Fe_{0.5}O_{3-\delta}$ ($x = 0.2, 0.5, 0.8$).

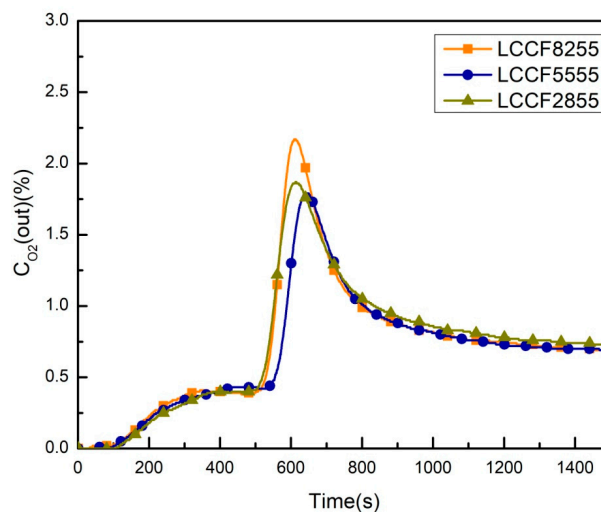
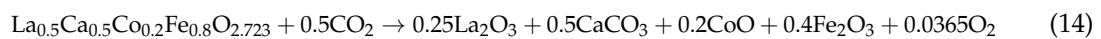
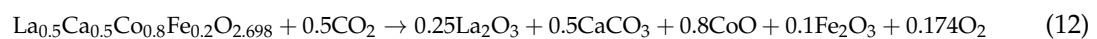
Sample	Oxygen Desorption Amount (mg O ₂ /g·sorbent)
LCCF8255	9.34
LCCF5555	8.81
LCCF2855	9.94

Table 3. Oxygen desorption amount of $\text{La}_{0.5}\text{Ca}_{0.5}\text{Co}_{1-y}\text{Fe}_y\text{O}_{3-\delta}$ ($y = 0.2, 0.5, 0.8$).

Sample	Oxygen Desorption Amount (mg O_2 /g·sorbent)
LCCF5582	10.71
LCCF5555	8.81
LCCF5528	8.50

As shown in Equations 9–11, oxygen desorption amounts of $\text{La}_{1-x}\text{Ca}_x\text{Co}_{0.5}\text{Fe}_{0.5}\text{O}_{3-\delta}$ with different Ca molar contents were almost the same.

Figure 7 and Table 3, respectively, illustrate the desorption curve and the oxygen desorption amount of $\text{La}_{0.5}\text{Ca}_{0.5}\text{Co}_{1-y}\text{Fe}_y\text{O}_{3-\delta}$ for different Fe molar contents. In this case, the adsorption temperature and desorption temperature were 800 °C and 850 °C, respectively. As shown in Figure 7, LCCF5582 exhibited a faster desorption rate and higher oxygen concentration during the desorption process. The maximum oxygen concentrations of the three candidates were 1.3%, 1.8%, and 2.4%, respectively. Comparing with A-site doping, B-site doping showed a more prominent effect on the oxygen desorption amount of perovskite-type sorbent at high temperature. This can be seen from the carbonation reaction equations as follows:

**Figure 7.** Oxygen desorption curves of $\text{La}_{0.5}\text{Ca}_{0.5}\text{Co}_{1-y}\text{Fe}_y\text{O}_{3-\delta}$ ($y = 0.2, 0.5, 0.8$).

As shown in Equations 12–14, the oxygen desorption amounts of $\text{La}_{0.5}\text{Ca}_{0.5}\text{Co}_{1-y}\text{Fe}_y\text{O}_{3-\delta}$ for different Fe molar contents were significantly different. Oxygen desorption amounts for different Fe molar contents of $\text{La}_{0.5}\text{Ca}_{0.5}\text{Co}_{1-y}\text{Fe}_y\text{O}_{3-\delta}$ are given in Table 3, where an Fe molar content of 0.2 resulted in an oxygen desorption value of 10.71 mg. This result agreed with the theoretical oxygen release amount that was obtained from the carbonation reaction equation.

3.4. Effect of A-/B-Site Doping on Performance of LCCF

The performance of LCCF with A-site doping was investigated. The oxygen non-stoichiometry δ and oxygen production amount are shown in Table 4. The δ of LCCF increased with an increasing Ca-doping amount. However, the oxygen desorption amount was nearly constant. This suggests

that different δ of LCCF via A-site doping did not play an important role for O_2 release amount. It is important to note that for permeation of the O_2 membrane of perovskites, oxygen non-stoichiometry δ is closely related to O_2 permeation properties. As A-site doping metal ions can increase the concentration of oxygen vacancies, oxygen ion conductivity can be created. Therefore, A-site doping had an obvious impact on δ of perovskite, while it contributed little to the O_2 release performance of LCCF. It can be concluded that the O_2 release amount of LCCF was not reliant on oxygen non-stoichiometry δ , which was generated from A-site doping.

Table 4. Effect of A-site doping on δ and performance of $La_{1-x}Ca_xCo_{0.5}Fe_{0.5}O_{3-\delta}$ ($x = 0.2, 0.5, 0.8$).

Effect of A-site Doping	δ	Oxygen Desorption Amount (mg O_2 /g·sorbent)
LCCF8255	0.119	9.34
LCCF5555	0.287	8.81
LCCF2855	0.47	9.44

The experimental results of LCCF with B-site doping are shown in Table 5. The oxygen non-stoichiometry δ of LCCF was nearly the same as B-site Fe-doping. However, Fe-doping had an obvious impact on the oxygen desorption amount, which was different from A-site Ca-doping. The oxygen desorption amounts decreased by increasing the Fe molar content. It is suggested that although B-site doping slightly affected the oxygen non-stoichiometry δ of $La_{1-x}Ca_xCo_{1-y}Fe_yO_{3-\delta}$, the O_2 desorption amount was closely linked to the B-site Fe molar content. Therefore, suitable B-site doping was necessary to obtain a higher O_2 amount. Table 6 summarizes the effect of A-/B-site doping on oxygen non-stoichiometry and performance of all $La_{1-x}Ca_xCo_{1-y}Fe_yO_{3-\delta}$ samples.

Table 5. Effect of B-site doping on δ and performance of $La_{0.5}Ca_{0.5}Co_{1-y}Fe_yO_{3-\delta}$ ($y = 0.2, 0.5, 0.8$).

Effect of B-site Doping	δ	Oxygen Desorption Amount (mg O_2 /g·sorbent)
LCCF5582	0.302	10.7
LCCF5555	0.287	8.81
LCCF5528	0.277	8.50

Table 6. Effect of A-/B-site doping on oxygen non-stoichiometry and performance of $La_{1-x}Ca_xCo_{1-y}Fe_yO_{3-\delta}$.

Samples	δ	Oxygen Desorption Amount (mg O_2 /g·sorbent)
LCCF5582	0.302	10.7
LCCF5555	0.287	8.81
LCCF5528	0.277	8.50
LCCF8255	0.119	9.34
LCCF2855	0.47	9.44

4. Conclusions

In this study, the oxygen non-stoichiometry δ and oxygen desorption performance of $La_{1-x}Ca_xCo_{1-y}Fe_yO_{3-\delta}$ (LCCF) with substitutions in A and B sites have been investigated. From this study, the following conclusions can be drawn:

1. The perovskite $La_{1-x}Ca_xCo_{1-y}Fe_yO_{3-\delta}$ (LCCF) sorbents with different A-/B-site doping amounts were synthesized by the liquid citrate method. XRD patterns indicate that all the samples have a perovskite structure with good crystallization. In addition, their tolerance factors are close to 1. The tolerance factor suggests that LCCF5582 has the most stable perovskite-type structure.

- The oxygen non-stoichiometry δ of LCCF sorbents was measured by iodometric titration. Oxygen non-stoichiometry values of LCCF by A-site doping increased with increasing Ca-doping amount, but the O₂ desorption amount was nearly constant. This suggests that the O₂ desorption amount is not dependent on the oxygen non-stoichiometry δ of LCCF from A-site doping.
- Oxygen non-stoichiometry values of LCCF with B-site Fe-doping are nearly the same. However, B-site Fe-doping has an obvious impact on the oxygen desorption amount. In addition, the oxygen desorption amounts increase with decreasing B-site Fe molar content. As a result, suitable B-site doping for perovskite is necessary to obtain a higher O₂ desorption amount.

Author Contributions: Conceptualization, Q.S.; methodology, S.L.; writing—original draft preparation, Q.S.; writing—review and editing, B.S. and J.Y.; supervision, G.Y.

Funding: This research was funded by National Natural Science Foundation of China, grant number 5160 6013 and 51779025.

Acknowledgments: The authors acknowledge the financial supports of National Natural Science Foundation of China (No.51606013, No.51779025).

Conflicts of Interest: The authors declare no conflict of interest.

Nomenclature

V_{O}	oxygen vacancy
O_{O}^{\times}	denote lattice oxygen
h^{\cdot}	electronic-hole
t	tolerance factors
LCCF2855	$\text{La}_{0.2}\text{Ca}_{0.8}\text{Co}_{0.5}\text{Fe}_{0.5}\text{O}_{3-\delta}$
LCCF5555	$\text{La}_{0.5}\text{Ca}_{0.5}\text{Co}_{0.5}\text{Fe}_{0.5}\text{O}_{3-\delta}$
LCCF8255	$\text{La}_{0.8}\text{Ca}_{0.2}\text{Co}_{0.5}\text{Fe}_{0.5}\text{O}_{3-\delta}$
LCCF5528	$\text{La}_{0.5}\text{Ca}_{0.5}\text{Co}_{0.2}\text{Fe}_{0.8}\text{O}_{3-\delta}$
LCCF5582	$\text{La}_{0.5}\text{Ca}_{0.5}\text{Co}_{0.8}\text{Fe}_{0.2}\text{O}_{3-\delta}$

References

- Shen, Q.W.; Zhang, Y.D.; Ding, H.R.; Xu, Y.Q.; Shi, B.C.; Zheng, Y.; Yuan, J.L. Performance and stability enhancement of perovskite-type nanomaterials applied for carbon capture utilizing oxyfuel combustion. *Energies* **2017**, *10*, 164. [[CrossRef](#)]
- Shen, Q.W.; Zheng, Y.; Luo, C.; Zheng, C.G. Development and characterization of $\text{Ba}_{1-x}\text{Sr}_x\text{Co}_{0.8}\text{Fe}_{0.2}\text{O}_{3-\delta}$ perovskite for oxygen production in oxyfuel combustion system. *Chem. Eng. J.* **2014**, *225*, 462–470. [[CrossRef](#)]
- Shen, Q.W.; Zheng, Y.; Li, S.A.; Ding, H.R.; Xu, Y.Q. Optimize process parameters of microwave-assisted EDTA method using orthogonal experiment for novel $\text{BaCoO}_{3-\delta}$ perovskite. *J. Alloys Compd.* **2016**, *658*, 125–131. [[CrossRef](#)]
- Yang, Q.; Lin, Y.S. Fixed-bed performance for production of oxygen-enriched carbon dioxide stream by perovskite-type ceramic sorbent. *Sep. Purif. Technol.* **2006**, *49*, 27–35. [[CrossRef](#)]
- Yang, Q.; Lin, Y.S.; Bulow, M. High temperature sorption separation of air for producing oxygen-enriched carbon dioxide stream. *AIChE J.* **2006**, *52*, 574–581. [[CrossRef](#)]
- Shen, Q.W.; Sun, L.N.; Wang, B.W. Numerical simulation of the effects of obstacles in gas flow fields of a solid oxide fuel cell. *Int. J. Electrochem. Sci.* **2019**, *14*, 1698–1712. [[CrossRef](#)]
- Liao, Q.; Chen, Y.; Wei, Y.Y.; Zhou, L.Y.; Wang, H.H. Performance of U-shaped $\text{BaCo}_{0.7}\text{Fe}_{0.2}\text{Ta}_{0.1}\text{O}_{3-\delta}$ hollow-fiber membranes reactor with high oxygen permeation for methane conversion. *Chem. Eng. J.* **2014**, *237*, 146–152. [[CrossRef](#)]
- Boldrini, S.; Mortalo, C.; Fasolin, S. Influence of microwave-assisted pechini method on $\text{La}_{0.8}\text{Sr}_{0.2}\text{Ga}_{0.83}\text{Mg}_{0.17}\text{O}_{3-\delta}$ Ionic Conductivity. *Fuel Cells* **2012**, *12*, 54–60. [[CrossRef](#)]
- Zheng, J.Q.; Zhu, Y.J.; Xu, J.S. Microwave-assisted rapid synthesis and photocatalytic activity of mesoporous Nd-doped SrTiO_3 nanospheres and nanoplates. *Mater. Lett.* **2013**, *100*, 62–65. [[CrossRef](#)]

10. Guntuka, S.; Banerjee, S.; Farooq, S.; Srinivasan, M.P. A- and B-site substituted lanthanum cobaltite perovskite as high temperature oxygen sorbent. *Ind. Eng. Chem. Res.* **2008**, *47*, 154–162. [[CrossRef](#)]
11. Yang, Z.; Lin, Y.S. High-temperature sorption process for air separation and oxygen removal. *Ind. Eng. Chem. Res.* **2002**, *41*, 2775–2784. [[CrossRef](#)]
12. Lin, Y.S.; Maclean, D.L.; Zeng, Y. High Temperature Adsorption Process. U.S. Patent 6059858, 9 May 2000.
13. Mizusaki, J.; Yamauchi, S.; Fueki, K.; Ishikawa, A. Nonstoichiometry of perovskite type oxides $\text{La}_{1-x}\text{Sr}_x\text{CoO}_{3-\delta}$. *Solid State Ionics* **1984**, *12*, 19–124. [[CrossRef](#)]
14. Teraoka, Y.; Hua, H.M.; Furukawa, S. Oxygen permeation through perovskite-type oxides. *Chem. Lett.* **1985**, *11*, 1743–1746. [[CrossRef](#)]
15. Yang, Z.; Lin, Y.S.; Zeng, Y. A semi-empirical equation for oxygen non-stoichiometry of perovskite-type ceramics. *Solid State Ionics* **2002**, *150*, 245–254. [[CrossRef](#)]
16. Cherepanov, V.; Gavrilova, A.L.Y.; Aksenova, T.V. Synthesis, structure and oxygen nonstoichiometry of $\text{La}_{0.4}\text{Sr}_{0.6}\text{Co}_{1-y}\text{Fe}_y\text{O}_{3-\delta}$. *Prog. Solid State Chem.* **2007**, *35*, 175–182. [[CrossRef](#)]
17. Thursfield, A.; Metcalfe, I.S. The use of dense mixed ionic and electronic conducting membranes for chemical production. *Chem. Mater.* **2004**, *14*, 2475–2485. [[CrossRef](#)]
18. Chen, W.M.; Hong, W.; Geng, J.F. Iodometric titration for determining the oxygen content of samples doped with Fe and Co. *Phys. C* **1996**, *270*, 349–353. [[CrossRef](#)]
19. Yin, Q.; Kniep, J.; Lin, Y.S. Oxygen sorption and desorption properties of Sr–Co–Fe oxide. *Chem. Eng. Sci.* **2008**, *63*, 2211–2218. [[CrossRef](#)]
20. Shannon, R.D. Revised effective ionic radii and systematic studies of interatomic distances in halides and chalcogenides. *Acta Crystallogr. Sect. A* **1976**, *32*, 751–767. [[CrossRef](#)]



© 2019 by the authors. Licensee MDPI, Basel, Switzerland. This article is an open access article distributed under the terms and conditions of the Creative Commons Attribution (CC BY) license (<http://creativecommons.org/licenses/by/4.0/>).